

Enhancement of R123 pool boiling by the addition of hydrocarbons

M.A. Kedzierski*

National Institute of Standards and Technology, Bldg. 226, Rm B114, Gaithersburg, MD 20899, USA

Abstract

This paper presents pool boiling heat transfer data for 10 different R123/hydrocarbon mixtures. The data consisted of pool boiling performance of a GEWA-T[®] surface for pure R123 and for 10 dilute solutions of five different hydrocarbons: (1) pentane, (2) isopentane, (3) hexane, (4) cyclohexane, and (5) heptane with R123. The heat flux and the wall superheat were measured for each fluid at 277.6 K. A maximum ($19 \pm 3.5\%$) increase over the pure R123 heat flux was achieved with the addition of 0.5% mass isopentane to R123. Other mixtures of isopentane, pentane, hexane, and cyclohexane with R123 exhibited smaller maximums than that of the R123/isopentane (99.5/0.5) mixture. Presumably, a layer enriched in hydrocarbon at the heat transfer surface caused the heat transfer enhancement. Conversely, an R123/heptane (99.5/0.5) mixture and an R123/cyclohexane (99.5/0.5) mixture exhibited only degradations with respect to the pure component performance for all test conditions. Several characteristics of the hydrocarbons were examined to determine their influence on the boiling heat transfer performance: molecular weight, molecular structure, composition, surface tension, and vapor pressure. © 2000 Elsevier Science Ltd and IIR. All rights reserved.

Keywords: Heat transfer; Mass transfer; Pool boiling; Refrigerant; Mixture; R123; Hydrocarbon; Heat transfer coefficient

Amélioration de l'ébullition libre du R123 par l'ajout d'hydrocarbures

Résumé

Dans cet article, les auteurs présentent les données de transfert de chaleur lors de l'ébullition libre d'une surface GEWA-T[®] pour le R123 et 10 solutions diluées (en utilisant du R123) de cinq hydrocarbures : (1) pentane, (2) isopentane, (3) hexane, (4) cyclohexane, et (5) heptane. Le flux thermique et la surchauffe ont été mesurés pour chaque mélange à 277,6 K. Une augmentation maximale de $19\% \pm 3,5\%$ du flux thermique par rapport à celui de R123 pur a été obtenu par l'ajout d'isopentane (à raison de 0,5 % m/v) au R123. D'autres mélanges de R123 avec de l'isopentane, du pentane, de l'hexane et du cyclohexane ont donné des valeurs maximales inférieures à celles du mélange R123 | isopentane (99,5 | 0,5). Ceci paraît être dû à une couche enrichie en hydrocarbure à la surface de transfert de chaleur, en raison de l'augmentation du transfert de chaleur. Inversement, un mélange de R123 | heptane (99,5 | 0,5) et un mélange R123 | cyclohexane (99,5 | 0,5) montraient des baisses seulement par rapport à R123 pur, pour toutes les conditions utilisées. On a examiné plusieurs caractéristiques des hydrocarbures (poids moléculaire, structure moléculaire, composition, tension superficielle, et pression de la vapeur) afin de déterminer leur influence sur le transfert de chaleur à l'ébullition. © 2000 Elsevier Science Ltd and IIR. All rights reserved.

Mots clés: Transfert de chaleur ; Transfert de masse ; Ebullition libre ; Frigorigène ; Mélange ; R123 ; Hydrocarbure ; Coefficient de transfert de chaleur

* Tel.: +1-301-775-5282; fax: +1-301-975-4032.

E-mail address: mark.kedzierski@nist.gov (M.A. Kedzierski)

Nomenclature

A_s	actual surface area (m)
E_{TW}	expanded uncertainty in the wall temperature (K)
E_q''	relative expanded uncertainty (%) in heat flux measurement
e	height of fin from tip to root (m)
k	thermal conductivity (W/m K)
L_y	length of test surface (m)
p	exterior perimeter of test surface (m)
q''	average wall heat flux (W/m ²)
Ra_L	Rayleigh number based on A_s/p
r_c	radius of cavity mouth (m)
S_f	spacing or gap between fin-tips (m)
s	estimate of standard deviation
T	temperature (K)
T_w	temperature of surface at root of fin (K)
U	expanded uncertainty
u_i	standard uncertainty
x	test surface coordinate (Fig. 2) (m)
y	test surface coordinate (Fig. 2) (m)

Greek symbols

ΔT	wall superheat: $T_w - T_s$ (K)
σ	surface-tension (kg/s ²)

Subscripts

h	hydrocarbon
l	liquid
m	mixture
p	pure R123
s	saturated state, solid surface
v	vapor

Superscripts

-	average
---	---------

Most of the work on liquid additives has been in surfactants for aqueous solutions [3–5]. Carey [6] and Rosen [7] describe how surfactants reduce the surface tension of water. Basically, the surfactant molecule must have polar and nonpolar ends, i.e. an amphiphathic structure. The nonpolar end of the surfactant distorts the interior structure of the solution. The structural distortion allows a surfactant molecule to travel to the liquid–vapor interface with less work than is required to bring a water molecule to the surface. By definition, the surface tension of the liquid–vapor interface is lowered when less work is required to bring a molecule to the surface.

Not much research has been done on surfactants for refrigerants. Kedzierski [8] measured a significant enhancement of R123 pool boiling with the addition of 1 and 2% hexane by mass to R123. He used the Gibbs adsorption equation and the Young and Dupre equation to speculate that the boiling heat transfer enhancement of R123 by the addition of hexane was caused by an accumulation of hydrocarbon at the boiling surface. In essence, the greater concentration of hydrocarbon or “excess layer” at the heat transfer surface caused a reduction of the surface energy between the solid surface and the liquid. The existence of an excess layer at the liquid–solid interface is analogous to the existence of a surfactant induced excess layer at a liquid–vapor interface. Consequently, the hydrocarbon is not a typical surfactant because it accumulates at the solid–liquid interface rather than the liquid–vapor interface. However, the reduction in the liquid–solid surface energy results in a similar reduction in bubble departure diameter that occurs with a conventional surfactant. As a consequence of the bubble size reduction, the active site density increases. A heat transfer enhancement existed when a favorable balance between an increase in site density and a reduction in bubble size occurs.

In the present study, five different hydrocarbons were tested as additives in various concentrations with R123 in an effort to investigate the enhancement mechanism of the excess layer. The various hydrocarbons were chosen for their wide range of properties: namely, normal boiling point, interfacial surface tension, molecular weight, and molecular structure. It was hypothesized that certain thermophysical and chemical properties of the hydrocarbon were favorable for the creation of an excess layer. For example, an R123/hydrocarbon mixture that behaved as an azeotrope in the bulk mixture would be more likely to exhibit a heat transfer enhancement with respect to pure R123. For an azeotropic mixture, the excess layer is formed due to the strong affinity of the hydrocarbon for the solid surface. Dilute solution of hydrocarbons with R123 and mixture of components with similar boiling points were unlikely to exhibit heat transfer degradations that can be associated

1. Introduction

Typically, binary mixtures exhibit a boiling performance degradation compared to their pure components [1,2]. Yet, some special liquids, when added in small quantities, enhance the boiling performance of pure fluids. For the refrigeration and air-conditioning industry, a liquid additive would be an economical means of reducing manufacturing and/or operating costs. For example, a liquid additive for 1,1-dichloro-2,2,2-trifluoroethane (R123) would enable existing water chillers to operate more efficiently or enable new water chillers to meet the same duty with fewer tubes. Unfortunately, liquid additives that significantly enhance refrigerant boiling performance are rare.

with concentration gradients. It was also believed that a large difference between the surface tension of the additive and the refrigerant would create a large potential to reduce the surface energy of the liquid–solid interface via the excess layer. The stability of the excess layer may rely on the molecular structure of the hydrocarbon. For example, a particular molecular structure of a hydrocarbon may be more conducive to the formation of an excess layer due to its degree of repulsion of the polar R123 molecules that are at the interface of the excess layer and the bulk liquid.

2. Apparatus

Fig. 1. shows a schematic of the apparatus that was used to measure the pool boiling data of this study. More specifically, the apparatus was used to measure the liquid saturation temperature (T_s), the average pool-boiling heat flux (q''), and the wall temperature (T_w) of the test surface at the root of the fin. The three principal components of the apparatus were test chamber, condenser, and purger. The internal dimensions of the test chamber were 25.4 mm × 257 mm × 1.54 m. The test chamber was charged with approximately 7 kg of R123 from the purger, giving a liquid height of approximately 80 mm above the test surface. As shown in Fig. 1, the test section was visible through two opposing, flat 150 × 200 mm quartz windows. The bottom of the test surface was

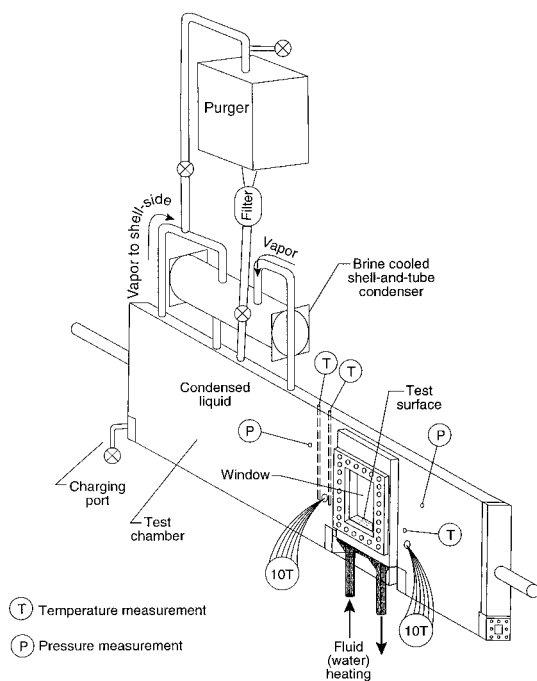


Fig. 1. Schematic of test apparatus.

Fig. 1. Schéma du banc expérimental.

heated with high velocity (2.5 m/s) water flow. The vapor produced by liquid boiling on the test surface was condensed by the brine-cooled, shell-and-tube condenser and returned as liquid to the pool by gravity.

To reduce the errors associated with the liquid saturation temperature measurement, the saturation temperature of the liquid was measured with two 450 mm long 1.6 mm diameter stainless steel sheathed thermocouples. The small diameter provided for a relatively rapid response time. Nearly the entire length of the thermocouple was in contact with either the test refrigerant vapor or liquid to minimize conduction errors. The tip of the two thermocouples were placed approximately 2 mm above and 150 mm (and 300 mm) to one side of the top of the test surface. This placement ensured that approximately 80 mm of the probe length was in relatively well-mixed liquid near the two-phase fluid above the test surface. To provide for a saturated liquid pool state, the mass of liquid in the pool was large compared to mass of liquid condensed. At the highest heat flux, it would require nearly 1 hour to evaporate and condense the entire test chamber charge. The lack of a temperature difference between the probe and the well-insulated, low emissivity, 38 mm aluminum test chamber walls essentially eliminated temperature errors due to radiation to the probe.

3. Test surface

Fig. 2 shows the oxygen-free high-conductivity (OFHC) copper GEWA-T[®] test plate used in this study. Commercially, flattening the tips of the GEWA-K[®] surface forms the GEWA-T[®] or “T-fin” surface. The GEWA-T[®] surface in this study was machined directly onto the top of the test plate by electric discharge machining (EDM). Fig. 3. shows a photograph of the fin surface. The gap between the fin-tips was 0.348 mm. The surface had approximately 667 fins per meter oriented along the short axis of the plate. The ratio of the surface area to the projected area of the surface was 2.47. The fin-tip width and the fin-height were 1.05 and 1.038 mm, respectively.

4. Measurements and uncertainties

The standard uncertainty (u_i) is the positive square root of the estimated variance u_i^2 . The individual standard uncertainties are combined to obtain the expanded uncertainty (U). The expanded uncertainty is commonly referred to as the law of propagation of uncertainty with a coverage factor. All measurement uncertainties are reported for a 95% confidence interval.

The copper–constantan thermocouples and the data acquisition system were calibrated against a glass-rod

standard platinum resistance thermometer (SPRT) and a reference voltage to a residual standard deviation of 0.005 K. The NIST Thermometry Group calibrated the fixed SPRT to two fixed points having expanded uncertainties of 0.06 mK and 0.38 mK. A quartz thermometer, which was calibrated with a distilled ice bath, agreed with the SPRT temperature to within approximately 0.003 K. Both the measured thermocouple electromotive force (EMF) and the measured 1 mV reference were regressed to the SPRT temperature. During a pool-boiling test, the 1 mV reference was measured prior to measuring each thermocouple EMF. The reference voltage was used to account for the drift in the acquisition mea-

surement capabilities over time. Before each test run, the measurements of a thermocouple in the bath with the SPRT were compared. The mean absolute difference between the thermocouple and the SPRT was 0.06 K over 1 year. Considering the fluctuations in the saturation temperature during the test and the standard uncertainties in the calibration, the expanded uncertainty of the average saturation temperature was no greater than 0.04 K. Consequently, it is believed that the expanded uncertainty of the temperature measurements was less than 0.1 K. The saturation temperature was also obtained from a pressure transducer measurement with an uncertainty of less than 0.03 kPa. The uncertainty of

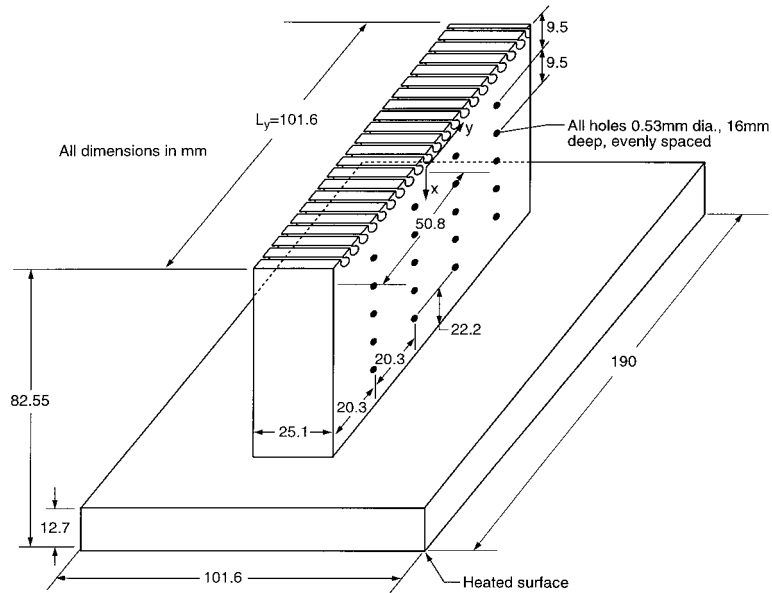


Fig. 2. OFHC copper GEWA-T[®] test plate and thermocouple coordinate system.

Fig. 2. Plaque d'essai GEWA-T[®] (en cuivre, hautement conductrice et sans oxygène) et système de thermocouple.

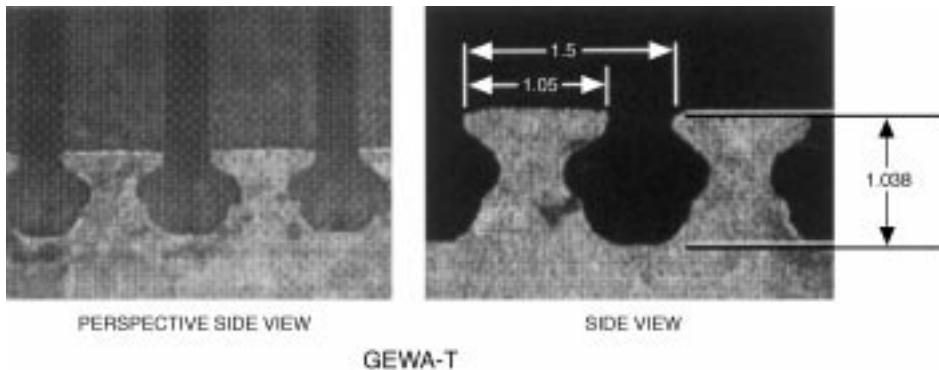


Fig. 3. Photograph of GEWA-T[®] geometry.

Fig. 3. Photo montrant la géométrie de GEWA-T[®].

the saturation temperature from a regression (with a residual standard deviation of 0.6 mK) of equilibrium data [9] for R123 was 0.17 K. The saturation temperature obtained from the thermocouple and the pressure measurement nearly always agreed within ± 0.17 K for the pure R123 data.

Fig. 2 shows the coordinate system for the 20 wells where individual thermocouples were force fitted into the side of the test plate. The wells were 16 mm deep to reduce conduction errors. Using a method given by Eckert and Goldstein [10], errors due to heat conduction along the thermocouple leads were estimated to be well below 0.01 mK. The origin of the coordinate system was centered on the surface with respect to the y -direction at the root of the fin. Centering the origin in the y -direction improved the accuracy of the wall heat flux and temperature calculations by reducing the number of fitted constants involved in these calculations. The x -coordinate measures the distance normal to the heat transfer surface. The y -coordinate measures the distance perpendicular to the x -coordinate. The thermocouples were arranged in four sets of five aligned in the x -direction. Following a procedure given by Kedzierski and Worthington [11], the size and arrangement of the thermocouple wells were designed to minimize the errors in the wall temperature and temperature gradient measurement.

The heat flux and the wall temperature were obtained by regressing the measured temperature distribution of the block to the governing two-dimensional conduction equation (Laplace equation). In other words, rather than using the boundary conditions to solve for the interior temperatures, the interior temperatures were used to solve for the boundary conditions following a backward stepwise procedure given in Kedzierski [12].

A backward stepwise regression was used to determine the best model or the significant terms of the solution to the Laplace equation in rectangular coordinates for each data point. Most infinite series solutions should converge within nine terms. The backward stepwise method began by regressing the first nine terms of the Laplace infinite series solution to the twenty measured plate temperatures:

$$T = A_0 + A_1x + A_2y + A_3(x^2 - y^2) + 2A_4xy + A_5x(x^2 - 3y^2) + A_6y(3x^2 - y^2) + A_7(x^4 - 6x^2y^2 + y^4) + 4A_8(x^3y - xy^3) \quad (1)$$

The above “full” model was reduced to its significant terms by removing terms with t -values less than two while maintaining the original residual standard deviation of the full model. Terms were removed one at a time. Regression of the 20 temperatures was done after each term with the smallest t -values was removed. Kedzierski [13] provides an overview of the various two-dimensional conduction models that were used to

reduce the measured temperatures to heat fluxes and wall temperatures.

Fourier’s law and the fitted constants (A_0, A_1, \dots, A_n) were used to calculate the average heat flux (q'') normal to and evaluated at the heat transfer surface as:

$$q'' \left(\frac{1}{L_y} \int_{-L_y/2}^{L_y/2} k \frac{\partial T}{\partial x} dy \right)_{x=0} = \bar{k} A_1 \quad (2)$$

where \bar{k} is the average thermal conductivity along the surface of the plate, and L_y is the length of the heat transfer surface as shown in Fig. 2.

The average wall temperature (T_w) was calculated by integrating the local wall temperature:

$$T_w = \left(\frac{1}{L_y} \int_{-L_y/2}^{L_y/2} T dy \right)_{x=0} = A_0 \quad (3)$$

Siu et al. [14] estimated the uncertainty in the thermal conductivity of OFHC copper to be about 2% to 3% by comparing round-robin experiments. Considering this, the relative expanded uncertainty in q'' was greatest at the lowest heat fluxes, approaching 10% of the measurement at 10 kW/m². In general, the $E_{q''}$ appears to be relatively constant between 6% and 3% for heat fluxes above 30,000 W/m². The average random error in the wall superheat — ($\Delta T_s = \bar{T}_w - T_s$) — was within 0.1 K. A more detailed discussion of the uncertainty analysis can be found in Kedzierski [15]. After the data was reduced, it was realized that only one of the two thermocouples used to measure the liquid saturation temperature was used to calculate the wall superheat. This oversight may have added approximately 0.05 K to the systematic error. Considering that the boiling curve may drift more than 0.05 K in a month due to surface aging, the shift in superheat was considered to be inconsequential due to the comparative purpose of the study.

5. Experimental results

The heat flux was varied from 80 to 10 kW/m² to simulate typical operating conditions of R123 chillers equipped with enhanced tubes. All pool boiling tests were taken at 277.6 K saturated conditions. The data were recorded consecutively starting at approximately 80 kW/m² and then descending to 10 kW/m² in intervals of approximately 4 kW/m². The descending heat flux procedure minimized the possibility of any hysteresis effects on the data, which would have made the data sensitive to the initial operating conditions. On average, 153 data points were measured for each fluid over 6 days. The measured heat flux and wall superheat for all of the data of this study are tabulated in Kedzierski [13].

The mixtures were prepared by first charging approximately 90% of the R123 into the test chamber to a known mass. Next, measured weights of the particular spectrophotometric grade hydrocarbon were injected through a valve in the side of the test chamber (see Fig. 1). The liquid hydrocarbon was injected with a syringe through the valve, followed by flushing with the remaining R123 charge. The flushing of R123 through the valve and connecting tubes also assisted in mixing the charge. All compositions are determined from the masses of the charged components and are given on a mass percent basis. The maximum uncertainty of the composition measurement is approximately 0.02%, e.g. the range of a 0.5% composition is between 0.48 and 0.52%.

The pool boiling performance of dilute mixtures of R123 and the following hydrocarbons were measured at 0.5 and 1.0% by mass hydrocarbon: isopentane, pentane, hexane, and cyclohexane. An R123/isopentane (99.5/0.5) by mass mixture was also tested along with an R123/heptane (99.9/0.1) by mass mixture. Pure R123 pool boiling data was taken to provide a baseline for comparison to the mixtures.

Fig. 4. presents the boiling curve for pure R123 at 277.6 K on the GEWA-T[®] surface. The boiling curve exhibits two characteristic regimes: a natural convection/boiling regime and a vigorous nucleate boiling regime. The regimes are separated by the cessation of vigorous nucleate boiling (CVNB). The CVNB occurs for the pure R123 data at approximately 9.5 K (24 kW/m²). The nucleate boiling regime exists for superheats that are greater than the CVNB condition. Here, the heat transfer is governed primarily by the formation of isolated bubbles within the fin cavities. The superheats below the CVNB are insufficient to support vigorous bubble generation. Consequently, natural convection

becomes a prevalent mode of heat transfer for superheats below CVNB. In this region, limited bubble activity exists.

Plots of the measured heat flux (q'') versus the measured wall superheat ($T_w - T_s$) for all of the fluids are given in Kedzierski [13]. On average, each fluid was tested over 6 days. For the most part, 1 day's test covered heat fluxes from 80 kW/m² to 10 kW/m². The solid line shown in Fig. 4 is a cubic best-fit regression or estimated mean of the data. Two cubic fits were required to cover the low and the high heat flux data. Table 1 gives the constants for the cubic regression of the superheat versus the heat flux for each test fluid. On average, the residual standard deviation of the low heat flux and the high heat flux data about the mean is 0.17 and 0.10 K, respectively. The dashed lines to either side of the mean represent the lower and upper 95% simultaneous (multiple-use) confidence intervals for the mean. The expanded uncertainty of the estimated mean wall superheat in the low heat flux region and the high heat flux region is approximately 0.1 and 0.07 K, respectively.

Fig. 4 compares the present R123 GEWA-T[®] boiling curve to R123 GEWA-T[®] boiling data that was taken approximately 5 years prior [8] to the present data in the same apparatus and for the same surface. The data differ substantially in the vigorous boiling region, but agree closely in the natural convection/boiling region. Apparently, the surface condition has changed such that many nucleation sites have been eliminated. The surface was stored in a felt-lined wooden box for the years between testing. The surface was cleaned prior to installation in the test apparatus with acetone, Tarnex[®], hot tap water, and acetone for both the 1993 and the present tests. Following the cleaning process, the surface was exposed to a heat lamp for several hours. Just prior to the present tests, the surface was used for active pool boiling testing for nearly two years after the storage period. Aging and/or fouling of the surface have produced an offset in the wall superheat of approximately 2 K. It is believed that the superheat offset is not caused by a malfunctioning of the test equipment because no equivalent offset between the measured saturation temperature and the saturation temperature obtained from the measured pressure was observed. Also, the agreement of low heat flux data for the two periods shows that the measurements are consistent. In addition, examination of the surface after the present tests revealed that it was fouled with a somewhat tacky substance. The surface may have been contaminated with decane from previous R123/decane pool boiling tests. The decane could have been adsorbed on the test surface in a manner similar to that, which was observed by Tamura et al. [16] where surfactants were irreversible adsorbed on metal surfaces.

Fig. 4 also compares the NIST 1993 GEWA-T[®] boiling curve to GEWA-TX[®] boiling curve measured by

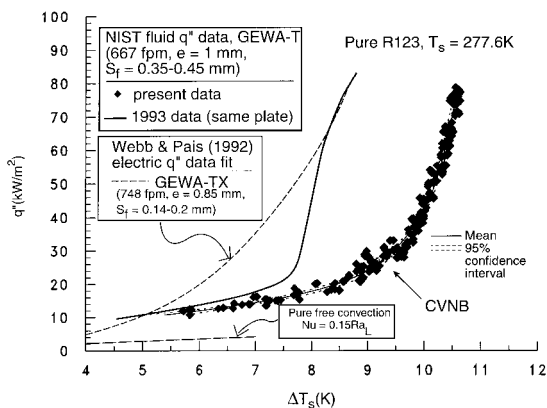


Fig. 4. R123 pool boiling curve for GEWA-T surface at 277.6 K.

Fig. 4. Courbe de l'ébullition libre pour la surface GEWA-T[®] à 277.6 K.

Table 1
 Constants for cubic curve fits for GEWA-T^{®a}

Tableau 1
 Courbe des constantes volumiques pour la GEWA-T[®]

Fluid		A_0	A_1	A_2	A_3
R123/isopentane (99.9/0.1)	$\Delta T_s > 8.5$ K	5.162564	2.213069×10^{-4}	-3.305539×10^{-9}	1.794215×10^{-14}
	$\Delta T_s < 9.5$ K	3.242045	2.982389×10^{-4}	$-9.070653 \times 10^{-10}$	-7.87954×10^{-14}
R123/isopentane (99.5/0.5)	$\Delta T_s > 8$ K	6.596237	1.387433×10^{-4}	-1.89345×10^{-9}	9.752913×10^{-15}
	$\Delta T_s < 9.5$ K	-1.953420	1.143663×10^{-3}	-4.152663×10^{-8}	5.346848×10^{-13}
R123/isopentane (99/1)	$\Delta T_s > 0$ K	6.239937	1.715029×10^{-4}	-2.614962×10^{-9}	1.441917×10^{-14}
	$\Delta T_s < 10$ K	-5.436468	1.228280×10^{-3}	-3.369096×10^{-8}	3.120554×10^{-13}
R123/pentane (99.5/0.5)	$\Delta T_s > 9.7$ K	8.725847	5.269372×10^{-5}	$-5.821089 \times 10^{-10}$	2.857575×10^{-15}
	$\Delta T_s < 9.7$ K	9.454738×10^{-1}	4.434199×10^{-4}	-1.626985×10^{-9}	$-1.148459 \times 10^{-13}$
R123/pentane (99/1)	$\Delta T_s > 9$ K	6.665111	1.609068×10^{-4}	-2.494825×10^{-9}	1.396698×10^{-14}
	$\Delta T_s < 9$ K	5.494870	-5.514591×10^{-4}	6.175966×10^{-8}	$-1.360361 \times 10^{-12}$
R123/hexane (99.5/0.5)	$\Delta T_s > 9$ K	7.052807	1.128998×10^{-4}	-1.337031×10^{-9}	6.112061×10^{-15}
	$\Delta T_s < 9$ K	2.307429	7.110618×10^{-5}	2.923709×10^{-8}	$-8.785910 \times 10^{-13}$
R123/hexane (99/1)	$\Delta T_s > 9.5$ K	8.415715	4.340422×10^{-5}	$-1.416185 \times 10^{-10}$	$-6.081541 \times 10^{-16}$
	$\Delta T_s < 9.5$ K	-8.193729	1.975566×10^{-3}	-7.828415×10^{-8}	1.061641×10^{-12}
R123/heptane (99.5/0.5)	$\Delta T_s > 10$ K	7.642573	1.367339×10^{-4}	-1.968117×10^{-9}	1.071097×10^{-14}
	$\Delta T_s < 10.7$ K	-4.695406×10^{-1}	8.135101×10^{-4}	-2.198312×10^{-8}	2.182051×10^{-13}
R123/cyclohexane (99/1)	$\Delta T_s > 9$ K	5.140536	2.582199×10^{-4}	-4.229872×10^{-9}	2.413322×10^{-14}
	$\Delta T_s < 9$ K	-3.819449	1.137466×10^{-3}	-2.584559×10^{-8}	2.736247×10^{-15}
R123/cyclohexane (99.5/1)	$\Delta T_s > 0$ K	3.727304	3.204812×10^{-4}	-5.075217×10^{-9}	2.809359×10^{-14}
R123	$\Delta T_s > 9$ K	6.21063	1.71370×10^{-4}	-2.475810×10^{-9}	1.287840×10^{-14}
	$\Delta T_s < 9.7$ K	-3.71984	1.21909×10^{-3}	-3.952890×10^{-8}	4.497650×10^{-13}

^a $\Delta T_s = A_0 + A_1 q'' + A_2 q''^2 + a_3 q''^3$; ΔT_s in Kelvins and q'' in W/m^2 .

Webb and Pais [17] at equal saturation temperatures. The figure summarizes the geometrical differences between the plate tested in this study and the tube that Webb and Pais [17] tested. The Webb and Pais (1992) GEWA-TX[®] data agree with the 1993 data for heat fluxes above 64 kW/m^2 and at 10 kW/m^2 and is greater than the present data for intermediate heat fluxes. The maximum percent difference between the two data sets of 100% occurs at the CVNB.

The greater performance of the Webb and Pais [17] GEWA-TX[®] surface compared to the 1993 NIST data for the intermediate heat flux region was partly due to the greater fins-per-meter (fpm) and the additional notch enhancement of the GEWA-TX[®] surface. Also, the gap between the fins (S_f) on the plate was significantly larger than that on the GEWA-TX[®] tube. The smaller fin-gap and the notch are effective at enhancing heat transfer at low site densities. A narrower fin-gap encourages bubble coalescence within the cavity. The notch acts to increase the site density. As the site density increases with the heat flux and the surface becomes saturated with bubbles, these geometry effects become less effective at heat transfer enhancement. Also, a flat plate does not experience the convection, as reported by Cornwell and Einarsson [18], that is induced by bubbles that slide within the channels of the side of a tube. The sliding bubbles also act to seed upper portions of the tube with vapor. These mechanisms would be less influ-

ential at higher heat fluxes where most of the potential sites have become active with vigorous bubble activity. Consequently, the performance difference between the plate and the tube becomes less significant at larger heat fluxes.

Fig. 4 also shows the predictions from a free convection correlation for a horizontal plate with the upper surface being heated which was recommended by Incropera and Dewitt [19]. Although the correlation is for a flat plate, it may be possible to account for the enhanced surface with the characteristic length defined as the surface area over the exterior perimeter of the plate. The predictions are substantially lower than the present measurements. This is consistent with the enhancement of the free convection by some nucleate boiling and the upward motion of bubbles.

Figs. 5–10 illustrate the effect of the addition of the various hydrocarbons to R123 on heat transfer performance. The figures plot the ratio of the mixture to the pure R123 heat flux (q''_m/q''_p) versus the pure R123 heat flux (q''_p) at the same wall superheat. A heat transfer enhancement exists where the heat flux ratio is greater than one and the 95% simultaneous confidence intervals (depicted by shaded regions) do not include the value one.

Fig. 5 shows that the R123/isopentane (99.5/0.5) mixture exhibits an enhancement for heat fluxes greater than approximately 24 kW/m^2 . The CVNB is located

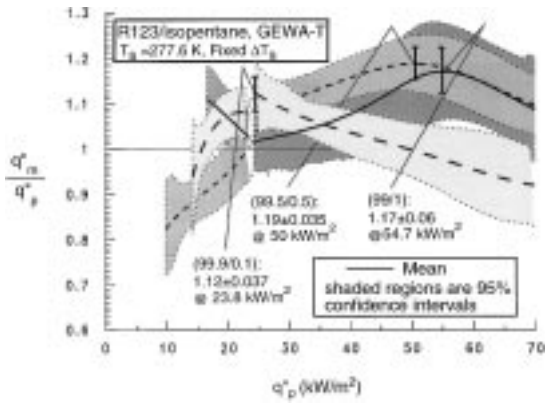


Fig. 5. Enhancement ratio for three dilute R123/isopentane mixtures.

Fig. 5. Taux d'amélioration pour les trois mélanges R123 / isopentane.

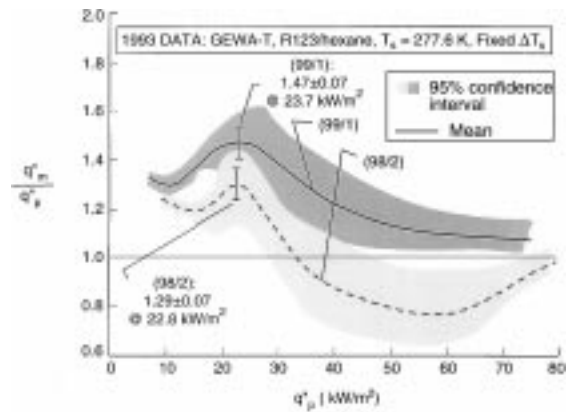


Fig. 8. Effect of hexane on R123 pool boiling heat flux as measured in 1993.

Fig. 8. Effet de l'hexane sur le flux thermique lors de l'ébullition libre du R123 (mesuré en 1993).

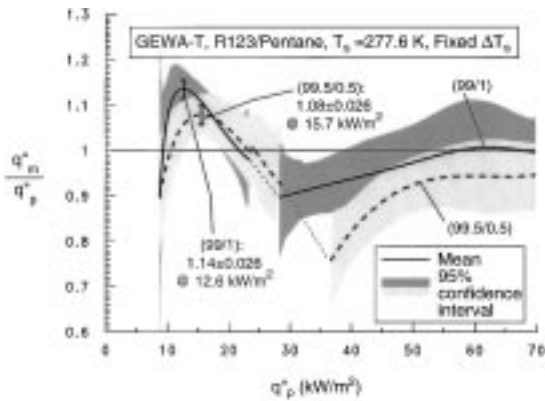


Fig. 6. Enhancement ratio for two dilute R123/pentane mixtures.

Fig. 6. Taux d'amélioration pour les deux mélanges R123 / pentane.

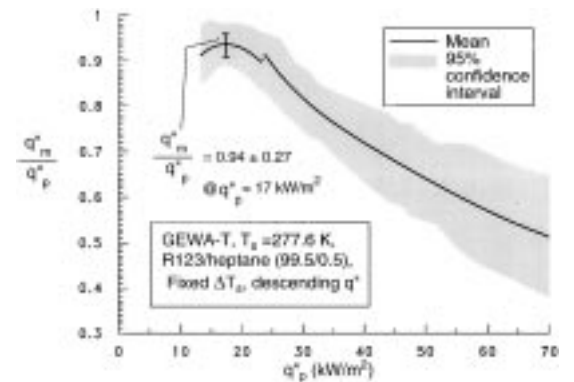


Fig. 9. Enhancement ratio for R123/heptane (99.5/0.5).

Fig. 9. Taux d'amélioration pour le mélange R123 / heptane (99,5 / 0,5).

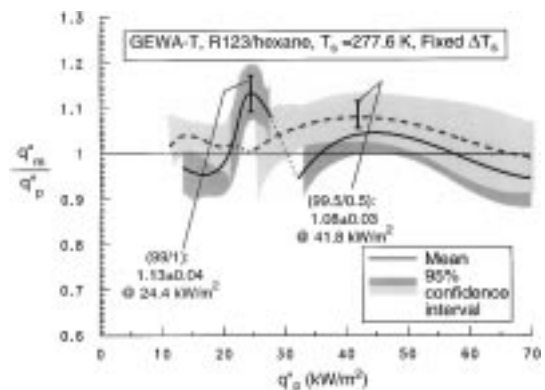


Fig. 7. Enhancement ratio for two dilute R123/hexane mixtures.

Fig. 7. Taux d'amélioration pour les deux mélanges R123 / hexane.

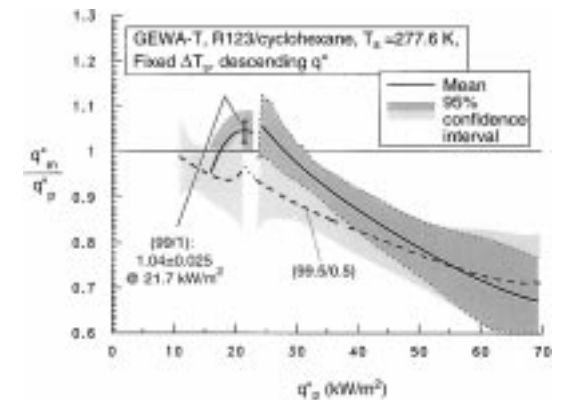


Fig. 10. Enhancement ratio for two dilute R123/cyclohexane mixtures.

Fig. 10. Taux d'amélioration pour les mélanges R123 / cyclohexane.

near 24 kW/m². Consequently, the addition of isopentane to R123 improves the heat transfer associated with vigorous boiling more so than it does for low-active-site-density boiling region. The maximum heat flux ratio for the 99.5/0.5 mixture was 1.19 at 50 kW/m². The average heat flux ratio for the R123/isopentane (99.5/0.5) mixture over the entire range of test heat fluxes was 1.10. The performance of the R123/isopentane (99/1) mixture is similar to that of the R123/isopentane (99.5/0.5) mixture but it has a higher uncertainty. The R123/isopentane (99.9/0.1) mixture shows a maximum near its CVNB and decreases for heat fluxes above the CVNB. For 99.5% confidence, no difference exists between the boiling performance of the 99.9/0.1 mixture and pure R123 for heat fluxes greater than 37 kW/m².

Fig. 6 shows that the R123/pentane (99.5/0.5) and (99/1) mixtures have similar heat flux ratio profiles. For example, both mixtures exhibit an enhancement for heat fluxes less than approximately 24 kW/m² and a degradation for heat fluxes greater than approximately 24 kW/m². Consequently, the addition of pentane to R123 enhances the low-active-site-density region rather than the vigorous boiling region. The maximum heat flux ratio for the R123/pentane (99/1) mixture was 1.14 at 12.6 kW/m². The average heat flux ratio for the R123/pentane (99/1) mixture over the entire range of test heat fluxes was 0.98. The performance of the R123/pentane (99.5/0.5) mixture is similar to that of the R123/pentane (99/1) mixture but slightly less over nearly the entire heat flux range. The R123/pentane (99.5/0.5) mixture had a maximum heat flux ratio of 1.08 and an overall average heat flux ratio of 0.94.

Fig. 7 shows the heat flux ratio for the R123/hexane (99.5/0.5) and R123/hexane (99/1) mixtures. The R123/hexane (99/1) mixture exhibits a maximum heat flux ratio of 1.13 in the low-active-site-density region at 24.4 kW/m², whereas the R123/hexane (99.5/0.5) mixture exhibits a maximum heat flux ratio of 1.08 in the vigorous nucleate boiling region (41.8 kW/m²). The average heat flux ratio for the entire test range was 1.04 and 1.01 for the R123/hexane (99.5/0.5) mixture and the R123/hexane (99/1) mixture, respectively. For 99.5% confidence, the R123/hexane (99.5/0.5) mixture boiling performance does not differ from that of pure R123 for heat fluxes greater than approximately 24 kW/m².

Fig. 8 shows data for an R123/hexane (99/1) mixture and an R123/hexane (98/2) mixture that were taken in 1993 [8] on the same surface and the same apparatus that was used in the present study. The R123/hexane (99/1) mixtures for the present study and the 1993 study exhibit a maxima at the same heat flux. However, the magnitude of the heat flux ratio for the 1993 study is much greater than that of the present study. Recall that Fig. 4 showed that the pure R123 boiling curve of the 1993 study significantly differed in the high heat flux region from the previous study. Obviously, the surface

characteristics of the GEWA-T[®] test plate were altered in the 5 years between the 1993 study and the present study. Presumably, the surface characteristics play a role in determining the effectiveness of the hydrocarbon in enhancing the active site density for nucleate boiling. From this, it is suspected that the heat flux ratios presented in this study would not be universally applicable to other enhancement geometries. However, the relative performance from additive to additive should be independent of fouling and the heat transfer geometry.

Fig. 9 shows that the addition of heptane by 5% mass to R123 causes a heat transfer degradation for heat fluxes from 15 to 70 kW/m². The maximum heat flux ratio for the R123/heptane (99.5/0.5) mixture is 0.94 and occurs at 17 kW/m². The heat flux ratio steadily decreases with increasing heat flux to approximately 0.51 at 70 kW/m².

Fig. 10 shows the heat flux ratio for two mixtures of R123 and cyclohexane. The R123/cyclohexane (99.5/0.5) mixture exhibits a heat transfer degradation as compared to pure R123 for the entire heat flux range of the tests. The R123/cyclohexane (99/1) has nearly the same performance of the (99.5/0.5) mixture with the exception of a small enhancement ($q''_m/q''_p = 1.04$) at $q''_p = 21.7$ kW/m².

6. Enhancement trends

The following five parameters were investigated for their influence on the boiling heat transfer performance of the hydrocarbon/R123 mixture: (1) the molecular weight of the hydrocarbon; (2) the difference in the boiling points of pure components at 39.8 kPa ($T_h - T_p$); (3) the difference in surface tension between the hydrocarbon and R123 at 277.6 K ($\sigma_h - \sigma_p$); (4) the mixture composition; and (5) the molecular structure of the hydrocarbon. Presumably, these parameters govern the dynamics of the formation of the excess layer for the R123/hydrocarbon mixtures. The mixtures should behave azeotropically in the bulk mixture. For very dilute solutions, mixtures may have large difference in normal boiling points while still maintaining azeotropic behavior [20]. However, due to its affinity for the solid, the hydrocarbon comes out of solution to form a confined region of higher hydrocarbon concentration at the wall. The initial formation of the excess layer due to the affinity of the hydrocarbon for the solid surface causes a composition shift past the azeotropic composition that may further increase the excess concentration through preferential boiling of the refrigerant. In addition, the excess layer cannot form on the wall unless the surface tension of the hydrocarbon is greater than that of R123. Otherwise, the hydrocarbon will act as a surfactant by accumulating at the liquid–vapor interface.

In Figs. 11–16 a linear model was used to provide only an approximate description of the trends in the

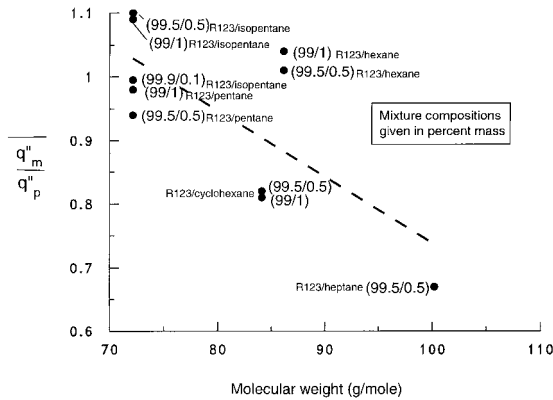


Fig. 11. Influence of molecular weight on the average enhancement ratio for dilute solutions of R123 and hydrocarbons.

Fig. 11. Influence du poids moléculaire sur le taux d'amélioration moyen pour les solutions diluées de R123 et d'hydrocarbures.

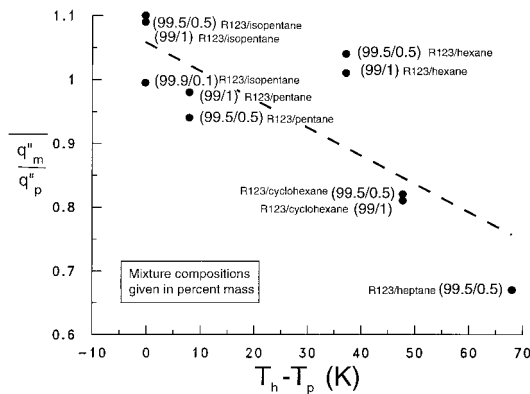


Fig. 12. Influence of boiling range on the average enhancement ratio for dilute solutions of R123 and hydrocarbons.

Fig. 12. Influence de l'éventail d'ébullition sur le taux d'amélioration moyen des solutions diluées de R123 et d'hydrocarbures.

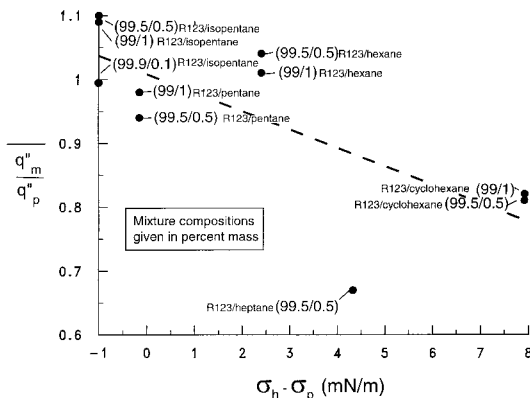


Fig. 13. Influence of surface tension on the average enhancement ratio for dilute solutions of R123 and hydrocarbons.

Fig. 13. Influence de la tension superficielle sur le taux d'amélioration moyen des solutions diluées de R123 et d'hydrocarbures.

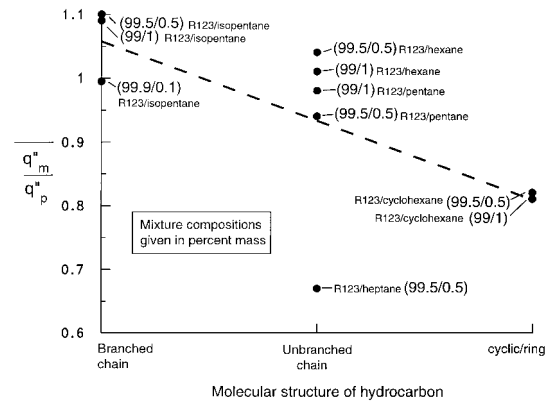


Fig. 14. Influence of molecular structure of hydrocarbon on the average enhancement ratio for dilute solutions of R123 and hydrocarbons.

Fig. 14. Influence de la structure moléculaire de l'hydrocarbure sur le taux d'amélioration moyen des solutions diluées de R123 et d'hydrocarbures.

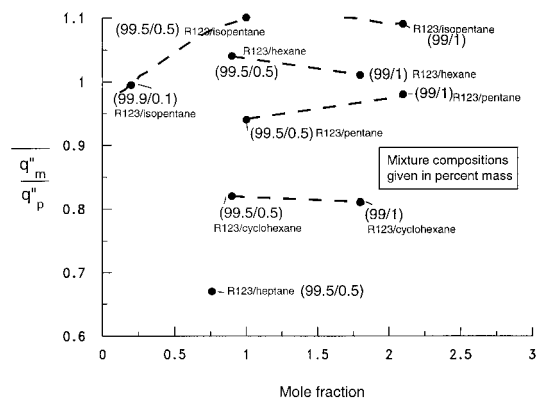


Fig. 15. Influence of mol fraction on the average enhancement ratio for dilute solutions of R123 and hydrocarbons.

Fig. 15. Influence de la fraction moléculaire sur le taux d'amélioration moyen des solutions diluées de R123 et d'hydrocarbures.

data. Consequently, nearly each plot contains one or two influential points [21] that may be considered outliers for the linear model. Future research might focus on gathering more data to better describe these trends and to identify the cause of outliers from the apparent linear trends.

Fig. 11 shows the heat flux ratio as a function of the molecular weight of the hydrocarbon in the R123/hydrocarbon mixture. In general, larger heat flux ratios are obtained for R123/hydrocarbon mixtures that have hydrocarbons with smaller molecular weights. Hydrocarbons with large molecular weights tend to “be sticky” or have a strong affinity for the solid surface. For this case, the thickness of the excess layer may act as fouling rather than a surfactant for the surface.

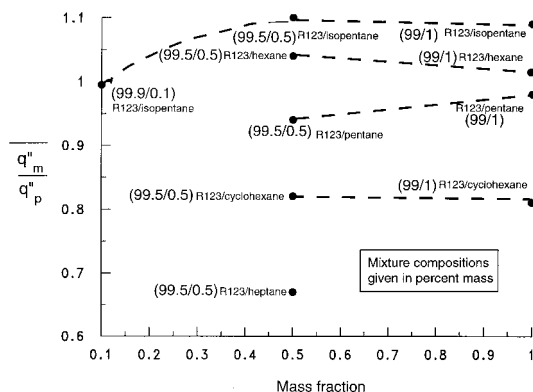


Fig. 16. Influence of mass fraction on the average enhancement ratio for dilute solutions of R123 and hydrocarbons.

Fig. 16. Influence de la fraction massique sur le taux d'amélioration moyen des solutions diluées de R123 et d'hydrocarbures.

Also, hydrocarbons with large molecular weights tend to have larger vapor pressure differences relative to R123. Fig. 12 illustrates the same point with the difference in boiling points (at 277.6 K) rather than the molecular weight. An R123/hydrocarbon mixture with a large vapor pressure difference or difference in boiling points will more likely exhibit zeotropic behavior, which can lead to a degradation in the heat transfer [22]. For example, it is likely that the performance of the R123/heptane (99.5/0.5) mixture suffers due to concentration gradients in the liquid.

Fig. 13 provides the heat flux ratio as a function of the difference between the surface tension of the pure hydrocarbon (σ_h) and that of the pure R123 (σ_p) at 277.6 K. The figure shows that larger heat flux ratios are associated with smaller differences in surface tension between the hydrocarbon and R123. For a binary mixture, an excess layer is a consequence of differences in surface tension between the component liquids. An additive becomes a liquid–vapor surfactant if its surface tension is less than that of the solute. For this case, the additive accumulates (forms an excess layer) at the liquid–vapor interface and lowers its surface tension. Conversely, if the surface tension of the additive is greater than that of the solute, the additive forms an excess layer at the solid–liquid interface. Here, the surface energy between the liquid and solid is reduced by the presence of the excess layer on the liquid–solid interface. Closer examination of Fig. 12 shows that isopentane may lower the surface tension of the liquid–vapor interface, while the other hydrocarbons may lower the surface tension of the liquid–solid interface. An excess layer at the liquid–vapor interface or one at the liquid–solid interface would produce the same result by different means. That is, a reduction in the surface-tension of either the liquid–vapor or the liquid–solid interface causes a reduction in the bubble contact angle

which, in turn, can cause an enhancement of the heat transfer [8]. Nevertheless, the difference between the surface tension of isopentane and R123 may be within the uncertainty of its prediction. Consequently, it is possible that all of the hydrocarbons act on the liquid–solid interface.

Fig. 14 illustrates the influence of the molecular structure of the hydrocarbon on the heat flux ratio. Apparently, the structure of the hydrocarbon has little influence on the heat transfer performance of the mixture. There is insufficient data to substantiate that, in general, a branch-chain hydrocarbon will give the best heat transfer performance. Even though three different unbranched-chain hydrocarbons were tested, the data is inconclusive due to the divergence of the R123/heptane (99.5/0.5) data from the mean of the data. The molecular structure does not appear to be a primary factor in determining the influence of the additives on the R123 heat transfer performance.

Figs. 15 and 16 show that neither the mol fraction nor the mass fraction have much influence on the heat transfer performance of the R123/hydrocarbon mixture. The slopes of the data appear to vary randomly from mixture to mixture. Consequently, each R123/hydrocarbon pair has a unique composition for optimum heat transfer performance.

7. Conclusions

The pool boiling performance of R123 on a GEWA-T[®] surface was enhanced as much as $(19\% \pm 3\%)$ by adding 0.5% mass isopentane. Overall, the R123/isopentane (99.5/0.5) mixture exhibited a 10% heat transfer enhancement over the entire range of test heat fluxes. In addition, the R123/hexane (99.5/0.5) mixture showed an overall 4% and a maximum 13% heat transfer enhancement over pure R123. The pool boiling enhancement mechanism is presumably due to an accumulation of hydrocarbon at the boiling surface in the channels. Apparently, the excess layer reduces the surface-energy between the liquid and the heat transfer surface causing the production of small diameter bubbles. Smaller bubbles will induce higher site densities than larger bubbles. The site density is increased enough to more than compensate for the loss in bubble size and results in a net heat transfer enhancement.

The influence of several parameters on the pool boiling heat transfer of the R123/hydrocarbon mixtures was investigated. In general, larger heat flux ratios were obtained for R123/hydrocarbon mixtures than for hydrocarbons with smaller molecular weights. An R123/hydrocarbon mixture with a large difference in boiling points was more likely to exhibit zeotropic behavior, which led to a degradation in the heat transfer. Apparently, the structure of the hydrocarbon had little influence on the heat

transfer performance of the mixture. Neither the mole fraction nor the mass fraction had much influence on the heat transfer performance of the R123/hydrocarbon mixture for the small composition range that was investigated.

Acknowledgements

This work was jointly funded by NIST and the US Department of Energy (project no. DE-01-95CE23808.000 modification #A004) under Project Manager Esher Kweller. Thanks go to the following NIST personnel for their constructive criticism of the first draft of the manuscript: Dr. V. Payne, Mr. J. Gebbie, and Mrs. J. Land. The author would also like to express appreciation to G. Glaeser and S. Nolan for data collection. Furthermore, the author extends appreciation to Dr. E. Lagergren for consultations on the uncertainty analysis.

References

- [1] Shock RAW. Boiling in Multicomponent fluids In: Multi-phase science and technology, 1982, Vol. 1. Hemisphere Publishing Corp. 281–386.
- [2] Thome JR. Enhanced boiling heat transfer. New York: Hemisphere Publishing Corp, 1990. (chapter 9)
- [3] Jontz PD, Myers JE. The effect of dynamic surface tension on nucleate boiling coefficients. *AIChE Journal* 1960;6(1):34–8.
- [4] Shah BH, Darby R. The effect of surfactant on evaporative heat transfer in vertical film flow. *Int J Heat Mass Transfer* 1973;16:1889–903.
- [5] Wu W, Yang Y, Maa J. Enhancement of nucleate boiling heat transfer and depression of surface tension by surfactant additives. *J Heat Transfer* 1995;117:526–9.
- [6] Carey VP. Liquid–vapor phase-change phenomena. Washington (DC): Hemisphere, 1992.
- [7] Rosen MJ. Surfactants and interfacial phenomena. New York: John Wiley & Sons, 1978.
- [8] Kedzierski, M.A. Enhancement of R123 pool boiling by the addition of *n*-hexane. *Journal of Enhanced Heat Transfer* 1999;6(5).
- [9] Morrison G, Ward DK. Thermodynamic properties of two alternative refrigerants: 1,1-dichloro-2,2,2-trifluoroethane (R123) and 1,1,1,2-tetrafluoroethane (R134a). *Fluid phase Equilibria* 1991;62:65–86.
- [10] Eckert ERG, Goldstein RJ. Measurements in heat transfer, 9–11
- [11] Kedzierski MA, Worthington III JL. Design and machining of copper specimens with micro holes for accurate heat transfer measurements. *Experimental heat transfer* 1993;6:329–44.
- [12] Kedzierski MA. Calorimetric and visual measurements of R123 pool boiling on four enhanced surfaces (NISTIR 5732). Washington (DC): US Department of Commerce, 1995.
- [13] Kedzierski MA. Enhancement of R123 pool boiling by the addition of hydrocarbons (NISTIR 6244). Washington, (DC): US Department of Commerce, 1998.
- [14] Siu MCI, Carroll WL, Watson TW. Thermal conductivity and electrical resistivity of six copper-base alloys (NBSIR 76-1003. Washington (DC): US Department of Commerce, 1976.
- [15] Kedzierski MA. Enhancement of R123 pool boiling by the addition of *n*-hexane (NISTIR 5780). Washington (DC): US Department of Commerce, 1996.
- [16] Tamura J, Tse JT, Adamson AW. *J Japan Petrol Inst* 1983;26:309.
- [17] Webb RL, Pais C. Nucleate pool boiling data for five refrigerants on plain, integral-fin and enhanced tube geometries. *Int J Heat Mass Transfer* 1992;35(8):1893–904.
- [18] Cornwell K, Einarsson JG. The influence of fluid flow on nucleate boiling from a tube. Eurotherm Seminar No. 8, *Advances in Pool Boiling Heat Transfer*, Paderborn, FRG, 11–12 May 1989 p. 28–41.
- [19] Incropera FP, DeWitt DP. *Fundamentals of heat and mass transfer*. 2nd Ed. New York: John Wiley & Sons, 1985 p. 439.
- [20] Lunger BS, Shealy GS. Compositions of a hydrofluorocarbon and a hydrocarbon. *International Patent WO 94/18282*, 1994.
- [21] Belsley DA, Kuh E, Welsch RE. *Regression diagnostics: identifying influential data and sources of collinearity*. New York: Wiley, 1980.
- [22] Kedzierski MA, Kim JH, Didion DA. Causes of the apparent heat transfer degradation for refrigeration mixtures. In: Kim JH, Nelson RA, Hashemi A, editors. *Two-Phase Flow and Heat Transfer, HTD-Vol. 197*. New York: ASME, 1992. p. 149–58.